

Article

# Development of a Novel Magnetic Reactor Based on Nanostructured Fe<sub>3</sub>O<sub>4</sub>@PAA as Heterogeneous Fenton Catalyst

María Gamallo <sup>1</sup>, Lucía Fernández <sup>1</sup>, Carlos Vázquez-Vázquez <sup>2</sup> , Alfonso Fondado <sup>3</sup>, Jorge Mira <sup>3</sup> , Gumersindo Feijoo <sup>1</sup> and María Teresa Moreira <sup>1,\*</sup>

<sup>1</sup> Department of Chemical Engineering, School of Engineering, Universidade de Santiago de Compostela, 15782 Santiago de Compostela, Spain; maria.gamallo@usc.es (M.G.); luciaf.fernandez@usc.es (L.F.); gumersindo.feijoo@usc.es (G.F.)

<sup>2</sup> Laboratory of Magnetism and Nanotechnology, Institute of Technological Research, Universidade de Santiago de Compostela, 15782 Santiago de Compostela, Spain; carlos.vazquez.vazquez@usc.es

<sup>3</sup> Department of Applied Physics, Faculty of Physics, Universidade de Santiago de Compostela, 15782 Santiago de Compostela, Spain; a.fondado@usc.es (A.F.); jorge.mira@usc.es (J.M.)

\* Correspondence: maite.moreira@usc.es; Tel.: +34-881816792

Received: 10 December 2018; Accepted: 22 December 2018; Published: 28 December 2018



**Abstract:** With the recent development of nanotechnology, magnetic nanoparticles (mNPs) have received increasing attention as potential heterogeneous Fenton catalysts in wastewater treatment applications, as an alternative to the conventional Fenton process using dissolved iron salts. Due to their superparamagnetic properties, Fe<sub>3</sub>O<sub>4</sub> mNPs can be easily recovered and reused by applying a magnetic field. However, Fe<sub>3</sub>O<sub>4</sub> mNPs have a marked tendency to form aggregates in water, leading to a decrease in their catalytic yield. To overcome these limitations, this work explores the catalytic activity of Fe<sub>3</sub>O<sub>4</sub> coated with poly(acrylic acid) (Fe<sub>3</sub>O<sub>4</sub>@PAA) as stabilized Fenton heterogeneous nanocatalyst, in the degradation of C.I. Reactive Blue 19 (RB19). To maximize the catalytic potential of Fe<sub>3</sub>O<sub>4</sub>@PAA, an experimental design based on the Response Surface Methodology (RSM) has been developed to optimize the conditions of the Fenton process in terms of Fe<sub>3</sub>O<sub>4</sub>@PAA concentration (100–300 mg L<sup>-1</sup>) and H<sub>2</sub>O<sub>2</sub> dose (100–400 mg L<sup>-1</sup>). Based on the results obtained, a novel sequential batch reactor (SBR) coupled to an external magnetic separation system has been developed, guaranteeing the complete retention of the mNPs in the system. This system allows the reuse of Fe<sub>3</sub>O<sub>4</sub>@PAA for at least 10 consecutive cycles, with a successful decolorization of RB19 after 4 h of treatment.

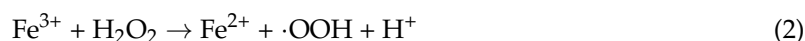
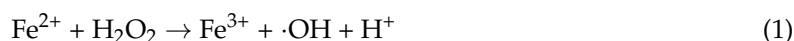
**Keywords:** magnetic separation unit; sequential batch reactor; Fe<sub>3</sub>O<sub>4</sub>@PAA; water treatment; Reactive Blue 19; Response Surface Methodology

## 1. Introduction

Advanced oxidation processes (AOPs) are wastewater treatment technologies based on the oxidation of pollutants by reactive oxygen species (ROS), mainly hydroxyl radicals ( $\cdot\text{OH}$ ). This type of powerful and unselective oxidants can attack nearly all organic complexes, leading to their decomposition. AOPs include photochemical methods, such as photocatalysis, photo-Fenton and the combination of ozone-hydrogen peroxide-ultraviolet radiation (O<sub>3</sub>/H<sub>2</sub>O<sub>2</sub>/UV), as well as non-photochemical methods, including ozonation, wet peroxide ozonation (O<sub>3</sub>/H<sub>2</sub>O<sub>2</sub>), catalytic ozonation and Fenton processes [1]. Due to the strong oxidative capacity of ROS, AOPs have been considered to treat different types of water bodies containing persistent pollutants, such as pharmaceuticals [2] and

personal care products [3] (PPCPs), endocrine disrupting compounds (EDCs) [4], dyes [5], or nitroaromatic explosives [6].

Among AOPs, Fenton catalysis is a well-known and simple technology, which has been shown to be more efficient in terms of operating costs for the degradation of a wide range of organic compounds at low and high concentrations [7,8]. The Fenton reaction starts with an electron transfer process, in which ferrous iron ( $\text{Fe}^{2+}$ ) reacts with hydrogen peroxide ( $\text{H}_2\text{O}_2$ ) to form  $\cdot\text{OH}$  (Equation (1)), so that it oxidizes organic matter, ideally resulting in complete mineralization to carbon dioxide ( $\text{CO}_2$ ) and water ( $\text{H}_2\text{O}$ ). The ferric iron ( $\text{Fe}^{3+}$ ) is then reduced to  $\text{Fe}^{2+}$  by  $\text{H}_2\text{O}_2$ , forming a hydroperoxyl radical ( $\cdot\text{OOH}$ ) (Equation (2)).



However, the conventional Fenton process has major drawbacks, the most notable being the impossibility of viable separation of the homogeneous catalyst ( $\text{Fe}^{2+}$ ) from the treated effluent and, therefore, the need for treatment of the ferric hydroxide sludge produced [9]. In this context, the cost associated with post-treatment can represent up to 50% of the total operating costs [10].

To overcome these impediments, the heterogeneous Fenton approach, using catalysts in solid phase that can be easily separated from the effluent, represents a promising alternative. However, heterogeneous catalysts have only a small fraction of iron on their surface, presenting slower reaction kinetics and mass transfer limitations compared to homogeneous catalysts [11,12]. The link between heterogeneous and homogeneous catalysts can be accomplished using nanostructured materials. Previous works have reported the use of engineered magnetic nanoparticles (mNPs), whose high surface/volume ratio compared to bulk materials enhances the contact between the reactants and the catalyst, making them efficient catalysts in water treatment applications (Zhang 2008, Sun 2013, Truskewycz 2016). Magnetite ( $\text{Fe}_3\text{O}_4$ ) is an environmentally benign material that contains Fe(II) and Fe(III) in its structure, and presents superparamagnetism when reduced to the nanoscale, allowing an easy and cost-effective recovery from the medium by simply applying an external magnetic field. This feature ensures a safe discharge of the treated effluent free of mNPs and the reuse of  $\text{Fe}_3\text{O}_4$  in a subsequent cycle, ideally without significant loss of catalytic activity [13,14]. However, the superparamagnetic nature of  $\text{Fe}_3\text{O}_4$  mNPs in aqueous media leads to interparticle interactions, causing the formation of large aggregates with lower surface/volume ratios, directly affecting their catalytic activity [15]. This shortcoming can be avoided by modifying the surface of mNPs with stabilizing agents, such as surfactants, silica or oleic acid derivatives, preventing mNPs from agglomeration by steric or electrostatic forces [16].

This study has focused on the use of poly(acrylic acid) (PAA) to coat the surface of  $\text{Fe}_3\text{O}_4$ , obtaining water-dispersible  $\text{Fe}_3\text{O}_4$ @PAA mNPs, as an improved heterogeneous Fenton agent with higher catalytic performance. The influence of the main operational variables (concentrations of  $\text{Fe}_3\text{O}_4$ @PAA mNPs and hydrogen peroxide) has been evaluated using the Surface Response Methodology (SRM) according to a central compound design, with the objective of parameterizing the optimal conditions to degrade C.I. Reactive Blue 19 (RB19). The selected dye belongs to the group of anthraquinones, widely used in the textile industry, being compounds resistant to light and oxidizing agents, mainly due to their highly stabilized resonance structure. Reactive dyes represent about 30% of the world production of synthetic dyes and are commonly released into environmental waters, causing damages not only to humans, but also to aquatic life [17], mainly associated with a decrease in light penetration and, therefore, photosynthetic activity, leading to oxygen deficiency [18,19].

Ensuring a long-term water treatment process and avoiding the release of mNPs into treated effluents are important concerns from an environmental perspective. With the goal of guaranteeing the complete retention of the nanocatalyst within the reaction system, a novel external magnetic separation unit is proposed. The main advantage of this technology is the simplicity in the separation of the

nanocatalyst, since the unit requires a minimum investment in infrastructure and negligible energy cost, as opposed to the use of high energy-demanding electromagnets [20,21].

## 2. Results and Discussion

### 2.1. Characterization of $\text{Fe}_3\text{O}_4@PAA$

$\text{Fe}_3\text{O}_4@PAA$  mNPs were structurally characterized by X-ray diffraction patterns. The position and relative intensities of the peaks observed in Figure 1a indicate that the main crystalline phase present in the sample corresponds to magnetite (Joint Committee of Powder Diffraction Standards (JCPDS) card number 19-0629). Figure 1b shows the transmission electron microscope (TEM) micrograph of the  $\text{Fe}_3\text{O}_4@PAA$  mNPs. The mNPs sample presented a regular, almost spherical morphology, with a size distribution of  $10.1 \pm 2.4$  nm. The total solid content was determined by thermogravimetry (TGA), obtaining a mNPs concentration of 2.05% by weight in the stock solution.

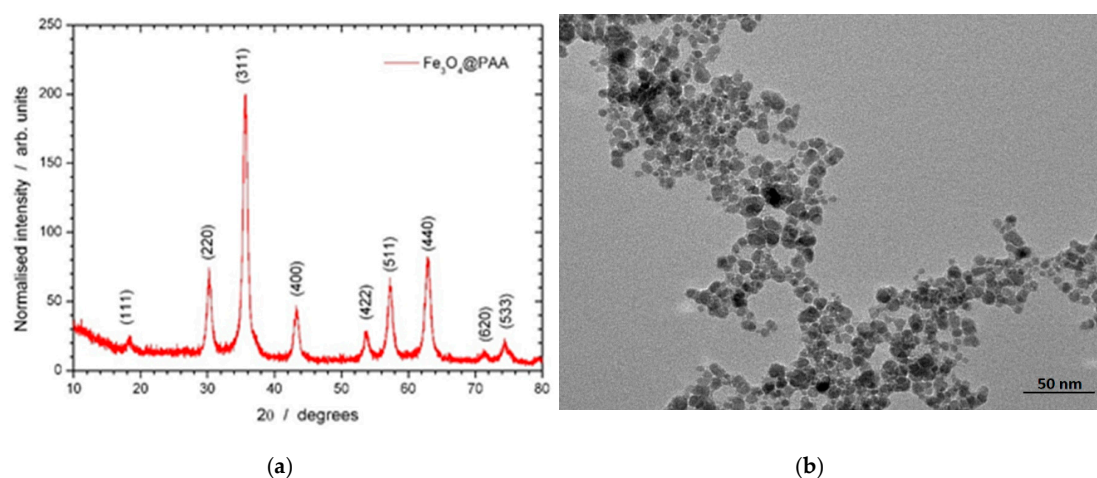


**Figure 1.** X-ray diffraction (XRD) pattern of  $\text{Fe}_3\text{O}_4@PAA$  mNPs. The corresponding Miller indices from magnetite (Joint Committee of Powder Diffraction Standards (JCPDS) card number 19-0629) are also shown (a, left) and transmission electron micrograph (TEM) of  $\text{Fe}_3\text{O}_4@PAA$  mNPs (b, right).

Magnetization studies of mNPs were conducted by measuring the variation of the magnetization as a function of the applied magnetic field at 300 K. The obtained magnetization curve (Figure 2) confirms the superparamagnetic behaviour of the sample, with a magnetization at 10 kOe close to  $70 \text{ emu g}^{-1}$ .

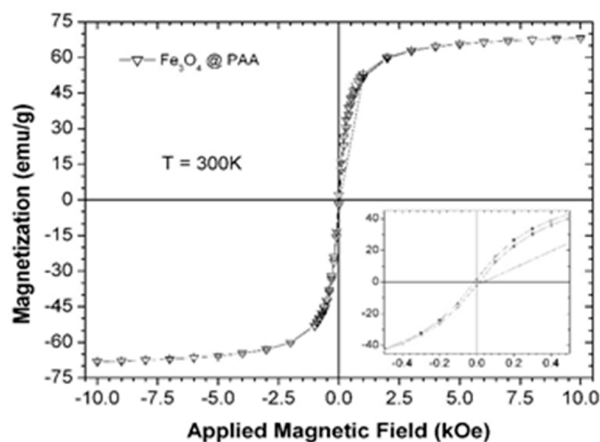


**Figure 2.** Variation of the magnetization with the applied magnetic field at 300 K of the  $\text{Fe}_3\text{O}_4@PAA$  mNPs.

## 2.2. Searching for Optimal Fenton Parameters for Dye Decolorization

The experimental results used for the optimization of the independent variables (mNPs and H<sub>2</sub>O<sub>2</sub> dose) are shown in Table 1.

**Table 1.** Factors and levels in the design matrix and data on the residual RB19 colour from experiments 1–11.

Exp No.	Dimensional Independent Variables		Dimensionless Independent Variables		Dependent Variable
	H <sub>2</sub> O <sub>2</sub> (mg L <sup>-1</sup> )	mNPs (mg L <sup>-1</sup> )	x1	x2	y1 or RB19 (%)
1	100	100	-1	-1	44.49
2	400	100	1	-1	37.79
3	100	300	-1	1	52.20
4	400	300	1	1	41.23
5	250	200	0	0	28.95
6	250	200	0	0	31.17
7	250	200	0	0	31.92
8	37.9	200	-1.414	0	52.69
9	250	341.4	0	1.414	45.04
10	462.1	200	1.414	0	38.06
11	250	58.6	0	-1.414	39.10

The suitability of the model was validated through the value of the determination coefficient ( $R^2 = 0.99$ ) and the significance value of the test F, obtained from the analysis of variance (ANOVA) analysis (89.97). Additionally, it was confirmed that the concentrations of mNPs and H<sub>2</sub>O<sub>2</sub> have a significant effect on dye degradation at the 5% of significance level. According to the response surface graph built on these data, the most efficient RB19 removal yields by the heterogeneous Fenton process reached values around 70% after 2 h of treatment (Figure 3). Optimal operating ranges were determined between 220 and 240 mg L<sup>-1</sup> of mNPs and between 190 and 235 mg L<sup>-1</sup> of H<sub>2</sub>O<sub>2</sub>, obtaining maximum dye decolorization (70.4%) with 230 mg L<sup>-1</sup> of Fe<sub>3</sub>O<sub>4</sub>@PAA mNPs and 220 mg L<sup>-1</sup> of H<sub>2</sub>O<sub>2</sub>. In view of the results obtained, it can be noted that an insufficient concentration of H<sub>2</sub>O<sub>2</sub> (<190 mg L<sup>-1</sup>) leads to a decrease in the effectiveness of RB19 removal due to the reduction of hydroxyl radicals generated, while high doses of H<sub>2</sub>O<sub>2</sub> above optimal concentrations (>235 mg L<sup>-1</sup>) can destroy the in situ formed ·OH radicals acting as scavenger itself (Equation (3)) [22].



The concentration of mNPs also has a significant effect on the catalytic efficiency. With increasing concentrations of Fe<sub>3</sub>O<sub>4</sub>@PAA mNPs between 100 and 220 mg L<sup>-1</sup>, RB19 removal increased, as the number of active sites in the catalyst is higher, which intensifies the production of hydroxyl radicals. However, this phenomenon occurs to a certain extent, obtaining that above 240 mg L<sup>-1</sup> of Fe<sub>3</sub>O<sub>4</sub>@PAA mNPs, catalytic efficiency decreases. A high concentration of mNPs can produce not only the agglomeration of nanoparticles, leading to a reduction in the effective surface area, but also the behaviour of Fe<sub>3</sub>O<sub>4</sub>@PAA mNPs acting as ·OH scavenger species (Equation (4)) [23].



In relation to RB19 concentration, dye decolorization in the range of 25–100 mg L<sup>-1</sup> was investigated using optimal operation conditions (230 mg L<sup>-1</sup> of Fe<sub>3</sub>O<sub>4</sub>@PAA mNPs and 220 mg L<sup>-1</sup> H<sub>2</sub>O<sub>2</sub>). The kinetic parameters were determined by adjusting a pseudo first-order kinetic model (Equation (5)).

$$\ln\left(\frac{C_t}{C_0}\right) = -k_{obs}t \quad (5)$$

where  $k_{obs}$  is the observed rate constant (h<sup>-1</sup>) and  $t$  is the time (h).

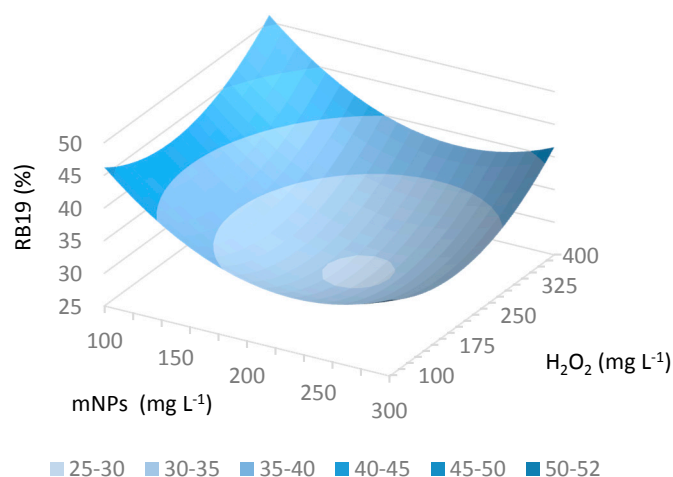


**Figure 3.** 3D plot showing the effect of the concentration ( $\text{mg L}^{-1}$ ) of hydrogen peroxide ( $\text{H}_2\text{O}_2$ ) and catalyst (mNPs) on the colour removal of RB19.

Table 2 shows the correlation coefficients ( $R^2$ ), the apparent constants of pseudo-first order rate ( $k_{obs}$ ) and the half-life times ( $t_{1/2}$ ). The fittings of the experimental data to this kinetic model are presented in Figure 4. After 2 h of treatment, RB19 decolorization decreased from 59.6 to 29.2% with the increase of the dye concentration from 50 to 100  $\text{mg L}^{-1}$ . Accordingly, the kinetic constant decreased from 0.408 to 0.117  $\text{h}^{-1}$ . Similar findings of RB19 removal have been previously reported [24,25]. On the other hand, it was found that the percentage of RB19 removal determined in the batch experiment with  $[\text{RB}]_0 = 25 \text{ mg L}^{-1}$  (68.2%) matches the predicted value of the model (70.4%).

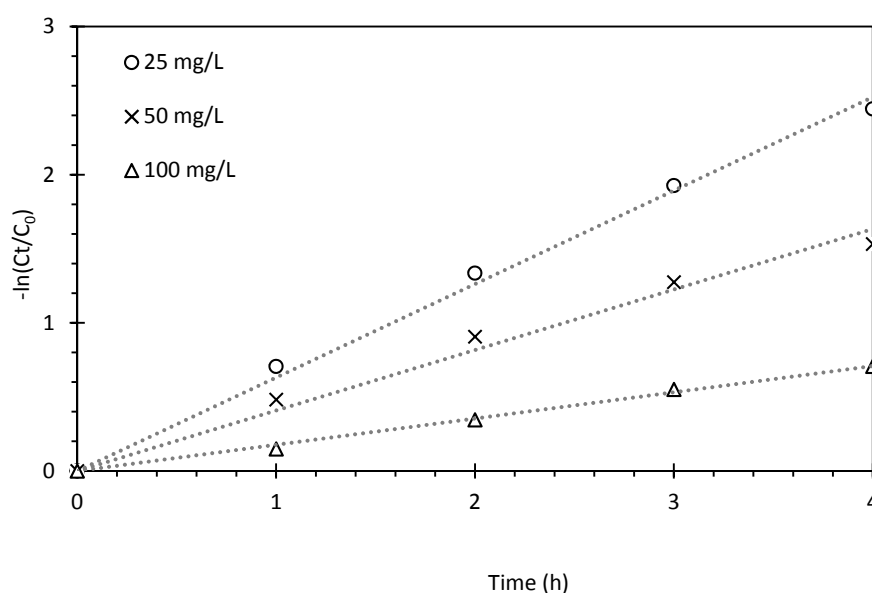


**Figure 4.** Pseudo-first-order reaction of RB19 decolorization at different initial dye concentrations (25–100  $\text{mg L}^{-1}$ ). Other conditions: 230  $\text{mg L}^{-1}$  of  $\text{Fe}_3\text{O}_4\text{@PAA}$  mNPs, 220  $\text{mg L}^{-1}$  of  $\text{H}_2\text{O}_2$ , pH 3.

### 2.3. Sequential Batch Reactor (SBR) with External Magnetic Separation System

The oxidative capacity of  $\text{Fe}_3\text{O}_4\text{@PAA}$  mNPs was independently evaluated in the degradation of RB19 under optimal operational parameters, in a 200 mL sequential batch reactor (SBR). The results depicted in Figure 5 show that the removal of RB19 in the reactor reached percentages of 74.7% after 2 h of treatment, and 91.3% after 4 h. To evaluate the influence of the mNPs coating, non-coated  $\text{Fe}_3\text{O}_4$  mNPs were used under the same operational conditions, obtaining removal rates of 43.6% and 73.4% after 2 h and 4 h, respectively, which demonstrates that the water stability provided by the PAA

coating greatly enhances the catalytic efficiency.  $\text{H}_2\text{O}_2$  control samples were conducted in the absence of  $\text{Fe}_3\text{O}_4@\text{PAA}$  mNPs, and no significant decolorization was observed after 4 h of reaction. Controls of RB19 adsorption onto mNPs in the absence of  $\text{H}_2\text{O}_2$  showed no significant removal (0.9%). In catalysis, pH is a key parameter that determines the interaction between the surface of the catalyst and the target compounds. Considering the dissociation constant of PAA ( $\text{pK}_a = 4.3$ ), the surface of the nanoparticle is neutral at pH 3, which explains that adsorption is negligible due to the absence of electrostatic forces.

**Table 2.** Pseudo-first-order kinetic rate constants ( $k_{\text{obs}}$ ), half-life time ( $t_{1/2}$ ) and regression coefficients ( $R^2$ ) for RB19 (25–100  $\text{mg L}^{-1}$ ) decolorization by heterogeneous Fenton.

Dye ( $\text{mg L}^{-1}$ )	$R^2$	$k_{\text{obs}}$ ( $\text{h}^{-1}$ )	$t_{1/2}$ (h)
25	0.995	0.631	1.098
50	0.983	0.408	1.698
100	0.996	0.177	3.909

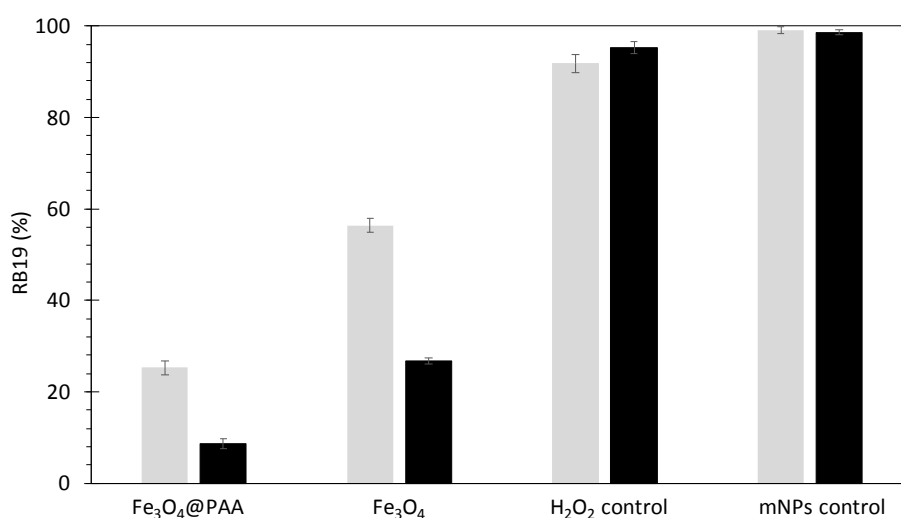


**Figure 5.** Residual RB19 colour percentage after 2 h (grey bars) and 4 h (black bars) of treatment by heterogeneous Fenton process ( $C_0 = 25 \text{ mg L}^{-1}$ ;  $\text{H}_2\text{O}_2 = 220 \text{ mg L}^{-1}$ ;  $\text{Fe}_3\text{O}_4@\text{PAA} = 230 \text{ mg L}^{-1}$ ).

The proposed pathway for RB19 degradation during the oxidation process in the presence of  $\cdot\text{OH}$  has been previously reported, suggesting an initial breakdown of the molecule by an attack on the C–N bond (Figure 6). Other mechanistic aspects would imply the cleavage of the quinone ring obtained in route (a), eventually to phthalic acid as final product, and the transformation of the sulfonate-transformation product obtained in route (b) [26].

Total organic carbon (TOC) analysis revealed that partial mineralization ( $22.7 \pm 4.0\%$ ) was obtained after 4 h of treatment. These results are consistent with previous studies in which the removal rate of RB19 involving only colour disappearance is faster than the complete cleavage of the chromophore. The characteristic blue colour of RB19 is owing primarily to a main absorption band in the visible region, with a maximum at 592 nm. RB19 is also present another intense band in the ultraviolet-A (UVA) region, corresponding to the anthraquinone structure [27].

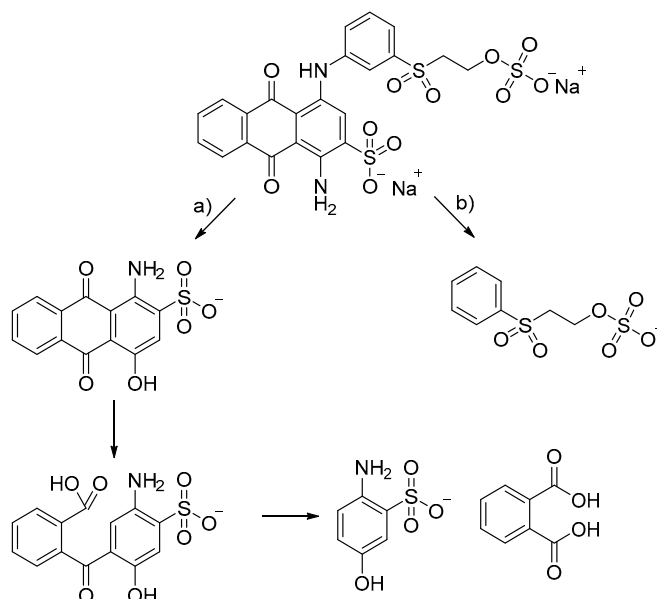


**Figure 6.** Proposed pathway of RB19 degradation by  $\cdot\text{OH}$  oxidation process [26].

The potential reuse of the catalyst was evaluated by conducting 10 cycles of RB19 decolorization (Figure 7). The process starts when the coloured influent is pumped into the reactor vessel, with a flow rate of  $600\text{--}750\text{ mL min}^{-1}$ , where the magnetic nanoparticles are in solution (Stage I). The reaction is allowed to be completed (Stage II) and, thereafter, the output stream of the reactor is pumped through the external magnetic separation unit, with a flow similar to the influent stream. The magnetic unit retains the nanoparticles and the treated effluent free of nanoparticle can be discharged (Stage III). Finally, a new contaminated influent is pumped back through the pipeline, dragging the retained nanoparticles back into the reactor, pushed by the inlet flow.

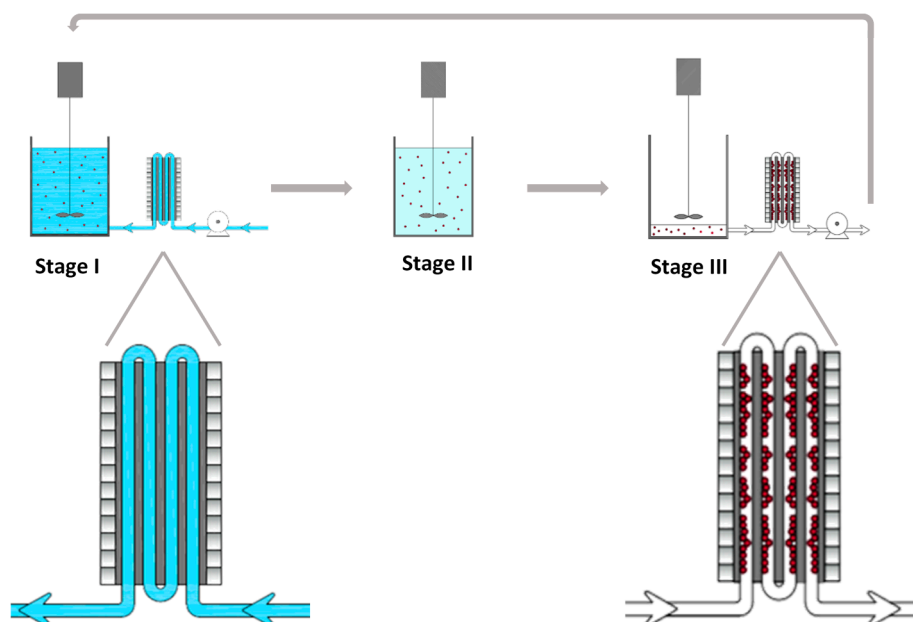


**Figure 7.** Reaction system scheme with external magnetic separation and its application in the treatment of coloured wastewater.

Although the mNPs are satisfactorily retained, the force exerted when feeding the inlet flow is sufficient to ensure that the retained NPs are returned to the reactor. This operational scheme is

repeated successively in different reaction cycles. The decolorization results obtained after each cycle were between 93.9 and 82.1% after 4 h of oxidative treatment (Figure 8).

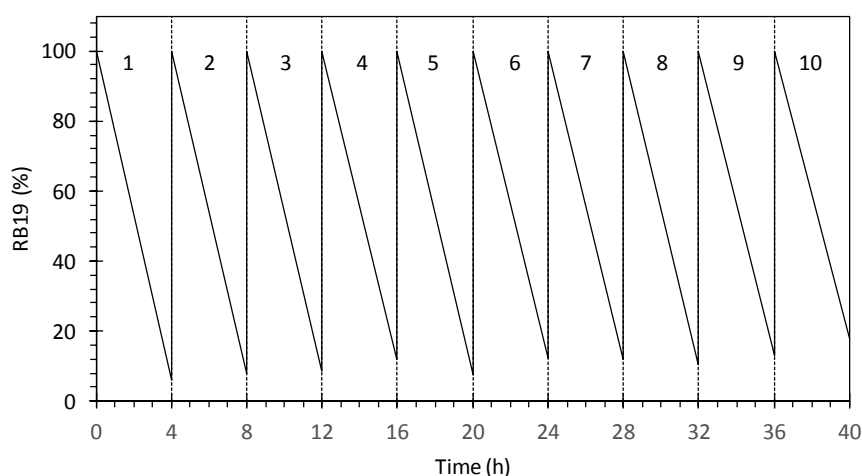


**Figure 8.** Decolorization of RB19 ( $C_0 = 25 \text{ mg L}^{-1}$ ) by heterogeneous Fenton ( $\text{H}_2\text{O}_2 = 220 \text{ mg L}^{-1}$ ;  $\text{Fe}_3\text{O}_4\text{@PAA} = 230 \text{ mg L}^{-1}$ ) process after 4 h of treatment in subsequent cycles.

It must be ensured that the external magnetic separation unit is fully effective to completely retain the nanocatalyst in the reaction system, avoiding in this way the discharge of mNPs into environmental waters. This separation unit presents an alternate arrangement of the magnets with face-to-face poles, in which the field lines extend to find the opposite pole, and consequently, the high gradient area is noticeably large (Figure 9). In the case of series arrangement, the magnetic field reaches high values only in the spaces between the individual magnets and at the top and bottom of the separation unit, so the retention of mNPs would be not so efficient. The results of  $\text{Fe}_3\text{O}_4\text{@PAA}$  reuse demonstrated the feasibility of applying these superparamagnetic nanocatalysts in successive cycles without affecting the properties of the material. Additionally, inductively coupled plasma-optical emission spectrometry (ICP-OES) analysis showed a Fe composition of 1.38 and 0.07% in the treated effluents of cycle 1 and 10, respectively.

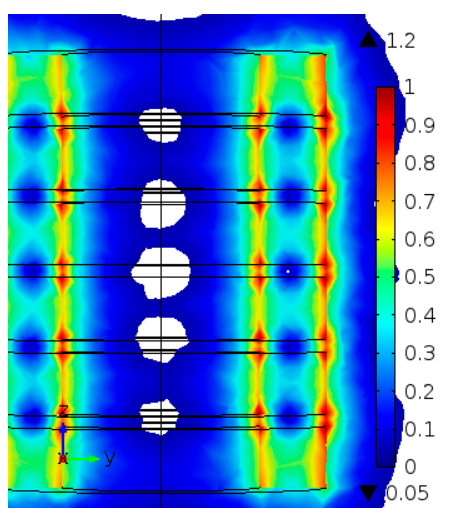


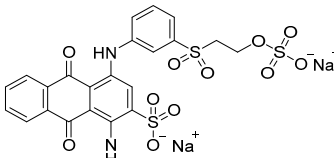
**Figure 9.** Modelling of magnetic fields (T) produced by alternate polarity configuration of magnets array.

### 3. Materials and Methods

#### 3.1. Chemicals and Magnetic Nanoparticles

All chemicals used in this research were reagent-grade without further purification steps. Hydrogen peroxide ( $\text{H}_2\text{O}_2$ ; 30 wt% in  $\text{H}_2\text{O}$ ) and C. I. Reactive Blue 19, also known as Remazol brilliant blue or disodium salt of 1-amino-2-sulfo-4-(3-sulfoxy-ethyl-sulfo-phenyl-1-ylamino)-5,10-anthraquinone (RB19;  $\text{MW} = 626.54 \text{ g mol}^{-1}$ ), were purchased from Sigma-Aldrich (St. Louis, MI, USA). The main physicochemical properties of the selected dye are summarized in Table 3. The stock solution of the dye ( $1 \text{ g L}^{-1}$ ) was prepared in double-distilled water and stored at  $4^\circ\text{C}$ .  $\text{Fe}_3\text{O}_4$ @PAA mNPs were supplied by Nanogap (Milladoiro, Spain). Sterically-stabilized  $\text{Fe}_3\text{O}_4$  nanoparticles were prepared by coprecipitation of Fe(II) and Fe(III) salts, following the Massart's method [28].

**Table 3.** Physicochemical characteristics of RB19.

Dye	Classification	Structure	$\lambda_{\text{max}}$	MW ( $\text{g mol}^{-1}$ )
Reactive Blue 19 (RB19)	Anthraquinone		592	626.54

#### 3.2. Characterization of $\text{Fe}_3\text{O}_4$ @PAA Magnetic Nanoparticles (mNPs)

The X-ray diffraction (XRD) study of the crystalline phases was carried out on powder samples using a Philips (Amsterdam, Holland) PW-1710 diffractometer (Cu  $\text{K}\alpha$  radiation source,  $\lambda = 1.54186 \text{ \AA}$ ). Measurements were performed in air at room temperature and collected in the  $2\theta$  angle range between  $10^\circ$  and  $80^\circ$ , with steps of  $0.02^\circ$  and 5 s per step. TEM images were taken with a JEOL JEM-1011 transmission electron microscope (Tokyo, Japan) operating at an accelerating voltage of 100 kV. One drop of a diluted sample solution was deposited on an amorphous carbon film in 400 mesh copper grids and allowed to evaporate at room temperature. The particle size distribution was performed by measuring the diameter of the nanoparticles with the ImageJ software. Thermogravimetric analysis (TGA) was conducted to estimate the concentration of the mNPs in dispersion. Thermogravimetric curves were recorded with a TA instruments TGA-Q500 (New Castle, Delaware, USA), operating under  $\text{N}_2$  atmosphere, with increasing temperature up to  $850^\circ\text{C}$ , at a scanning rate of  $10^\circ\text{C min}^{-1}$ . Magnetization curves as a function of the applied magnetic field (up to 10 kOe) for  $\text{Fe}_3\text{O}_4$ @PAA mNPs were obtained with a DMS Model 1660 Vibrating Sample Magnetometer (VSM), in dry samples at room temperature.

To determine the possible catalyst loss expressed as iron concentration ( $\text{mg L}^{-1} \text{ Fe}$ ) in the treated effluent after its application on RB19 removal, Fe was determined by ICP-OES with a Perkin-Elmer Optima 3300 DV equipped with an autosampler Perkin-Elmer AS91 (Waltham, MA, USA).

#### 3.3. Experimental Set-Up for Dye Removal by Heterogeneous Fenton Catalysis

Batch experiments were performed in 20-mL glass reactors containing 10 mL of an aqueous solution of RB19 ( $25 \text{ mg L}^{-1}$ ) and corresponding concentration of  $\text{Fe}_3\text{O}_4$ @PAA ( $100\text{--}300 \text{ mg L}^{-1}$ ) at pH 3. RB19 degradation was initiated by adding  $\text{H}_2\text{O}_2$  to the reaction medium. Then, samples were incubated at room temperature and continuous agitation at 150 rpm in an orbital shaker (C24 Incubator shaker, New Brunswick Scientific, NJ, USA). At regular intervals of time, aliquots ( $200 \mu\text{L}$ ) were taken after magnetic separation of the nanocatalyst from the treated solution, and absorbance measurements were performed on a BioTek PowerWave XS2 micro-plates spectrophotometer (Winooski, VT, USA) to

monitor the colour removal of RB19 ( $\lambda = 592$  nm). The decolorization yield (%) was determined as the extent of colour disappearance, calculated by Equation (6):

$$\text{Decolorization (\%)} = \frac{(C_0 - C_t)}{C_0} \times 100 \quad (6)$$

where  $C_0$  and  $C_t$  represent the dye concentration ( $\text{mg L}^{-1}$ ) before and after the reaction time, respectively. To clarify the influence of mNPs on dye removal, control experiments containing RB19 and  $\text{H}_2\text{O}_2$  were conducted in parallel experiments lacking catalyst.

where  $k_{\text{obs}}$  is the observed rate constant ( $\text{h}^{-1}$ ) and  $t$  is the time (h). A total organic carbon (TOC) analyser with autosampler (Shimadzu TOC 5000, Kyoto, Japan) was used to determine TOC concentrations in samples at  $\text{mg L}^{-1}$  levels and to calculate the percentage of mineralization after treatment.

### 3.4. Experimental Design and Optimization

Colour removal of RB19 ( $25 \text{ mg L}^{-1}$ ) by the heterogeneous Fenton process was evaluated following a factorial, centred second-order experimental design for the optimization of the main experimental conditions. The concentrations of  $\text{Fe}_3\text{O}_4\text{@PAA}$  mNPs ( $100\text{--}300 \text{ mg L}^{-1}$ ) and  $\text{H}_2\text{O}_2$  ( $100\text{--}400 \text{ mg L}^{-1}$ ) were selected as independent variables for the experimental design to obtain information, both single and combined, on their effect on the decolorization of RB19 (Table 4). The central composite design (CCD) contains the complete factorial design and star design at the five factor levels:  $-\alpha$ ,  $-1$ ,  $0$ ,  $1$  y  $\alpha$ , where  $|\alpha| = (2^f)^{1/4}$ , i.e., 1.414 in the case of two factors ( $f = 2$ ). Eleven series of batch experiments were carried out, and three replicates were conducted at the central point.

**Table 4.** Variables and levels applied to the RB19 decolorization through an experimental design of the Fenton process.

Variables	Levels				
	−1.414	−1	0	1	1.414
$\text{Fe}_3\text{O}_4\text{@PAA}$ mNPs ( $\text{mg L}^{-1}$ )	58.6	100	200	300	341.4
$\text{H}_2\text{O}_2$ ( $\text{mg L}^{-1}$ )	250	100	250	400	462.1

The experimental data were tested according to the proposed model using commercial IBM® SPSS Statistics® 20 software. To predict the decolorization percentage of the dye, the experimental data were fitted using a second-order polynomial equation described by the following mathematical model:

$$y_j = \beta_{0j} + \sum_{i=1}^2 \beta_{ij}x_i + \sum_{i=1}^2 \sum_{k=1}^2 \beta_{ikj}x_ix_k \quad (7)$$

where  $y_j$  is the dependent variable ( $j = 1$ ),  $\beta_{0j}$ ,  $\beta_{ij}$  and  $\beta_{ikj}$  are the regression coefficients calculated from the experimental results by the least-squares method, and  $x_i$  or  $x_k$  ( $k \geq i$ ) are the dimensionless, normalized independent variables.

### 3.5. Sequential Batch Reactor with Magnetic Separation System

The proof-of-concept in the operation of the sequential batch reactor with magnetic separation system was conducted in 200 mL batch experiments at room temperature and continuous stirring (150 rpm). The previously estimated optimal concentrations of mNPs and  $\text{H}_2\text{O}_2$  ( $230$  and  $220 \text{ mg L}^{-1}$ , respectively) were applied for the decolorization of RB19 ( $25 \text{ mg L}^{-1}$ ). Figure 7 shows the reaction system, in which the operating scheme of the reactor coupled to the magnetic separation unit is presented. The reactor was operated sequentially according to the fill-and-draw principle,

which consists of the following steps: fill, react, magnetic retention of the catalyst, and withdrawal of the reaction medium.

The external magnetic separation unit comprised a system of Teflon tubes (internal and external diameters of 2 and 5 mm, respectively), on which an external magnetic field was applied. This magnetic field was produced by a 10 ring-shaped neodymium-iron-boron (NdFeB; with the following dimensions of each of the toroidal magnets: inner diameter 16 mm, outer diameter 26.8 mm and length 5 mm). The toroidal magnets that make up the magnetic separation unit are permanently aligned and coupled with alternating polarity. Figure 9 shows a simulation of the axial cut of the magnetic arrangement, with a magnetic field in the range of 0.05 to 1.2 T.

#### 4. Conclusions

The present study investigated different operating conditions to optimize the removal of a recalcitrant compound (RB19) from aqueous media by heterogeneous Fenton catalysis, in order to overcome the limitations of conventional Fenton technology. The central composite design selected as a Response Surface Methodology allowed determination of the optimal conditions to perform dye degradation. From the outcomes of the analysis of RB19 decolorization, it was proven that nanocatalyst stabilization plays a crucial role. Fe<sub>3</sub>O<sub>4</sub>@PAA mNPs exhibit good structural stability and can be easily separated by a magnetic field. Furthermore, the reaction system coupled with a magnetic separation unit with minimal energy requirement, unlike electromagnets, is a promising approach to achieving high efficiency in the removal of organic microcontaminants through the recovery and complete reuse of nanocatalysts.

**Author Contributions:** Conceptualization: M.T.M., G.F., J.M., A.F. and C.V.V. Investigation: M.G. Writing-original draft preparation: M.G. and L.F. Writing-review and editing: M.T.M., C.V.V. and L.F.

**Funding:** This research was supported by two projects granted by Spanish Ministry of Science and Innovation: MODENA Project CTQ2016-79461-R and CLUSTERCAT Project MAT2015-67458-P, and Fundación Ramon Areces, Spain (Project CIVP18A3940). The authors belong to the Galician Competitive Research Groups ED431C-2017/22 and ED431C-2017/29, programme co-funded by FEDER, CRETUS Strategic Partnership (AGRUP2015/02) and AEMAT (ED431E 2018/08).

**Conflicts of Interest:** The authors declare no conflict of interest.

#### References

1. Bethi, B.; Sonawane, S.H.; Bhanvase, B.A.; Gumfekar, S.P. Nanomaterials-based advanced oxidation processes for wastewater treatment: A review. *Chem. Eng. Process.* **2016**, *109*, 178–189. [[CrossRef](#)]
2. Androzzzi, R.; Campanella, L.; Fraysse, B.; Garric, J.; Gonnella, A.; Lo Giudice, R.; Marotta, R.; Pinto, G.; Pollio, A. Effects of advanced oxidation processes (AOPs) on the toxicity of a mixture of pharmaceuticals. *Water Sci. Technol.* **2004**, *50*, 23–28. [[CrossRef](#)] [[PubMed](#)]
3. Tayo, L.L.; Caparanga, A.R.; Doma, B.T.; Liao, C.-H. A Review on the Removal of Pharmaceutical and Personal Care Products (PPCPs) using Advanced Oxidation Processes. *J. Adv. Oxid. Technol.* **2018**, *21*, 196–214. [[CrossRef](#)]
4. Ning, B.; Graham, N.; Zhang, Y.; Nakonechny, M.; Gamal El-Din, M. Degradation of Endocrine Disrupting Chemicals by Ozone/AOPs. *Ozone Sci. Eng.* **2007**, *29*, 153–176. [[CrossRef](#)]
5. Sathishkumar, P.; Mangalaraja, R.V.; Anandan, S. Review on the recent improvements in sonochemical and combined sonochemical oxidation processes—A powerful tool for destruction of environmental contaminants. *Renew. Sus. Energ. Rev.* **2016**, *55*, 426–454. [[CrossRef](#)]
6. Ayoub, K.; van Hullebusch, E.D.; Cassir, M.; Bermond, A. Application of advanced oxidation processes for TNT removal: A review. *J. Hazard. Mater.* **2010**, *178*, 10–28. [[CrossRef](#)] [[PubMed](#)]
7. Sable, S.S.; Ghute, P.P.; Álvarez, P.; Beltrán, F.J.; Medina, F.; Contreras, S. FeOOH and derived phases: Efficient heterogeneous catalysts for clofibric acid degradation by advanced oxidation processes (AOPs). *Catal. Today* **2015**, *240*, 46–54. [[CrossRef](#)]

8. Krishnan, S.; Rawindran, H.; Sinnathambi, C.M.; Lim, J.W. Comparison of various advanced oxidation processes used in remediation of industrial wastewater laden with recalcitrant pollutants. In Proceedings of the IOP Conference Series: Materials Science and Engineering, Beijing, China, 24–27 October 2017; p. 012089.
9. Álvarez, P.M.; Jaramillo, J.; López-Piñeiro, F.; Plucinski, P.K. Preparation and characterization of magnetic TiO<sub>2</sub> nanoparticles and their utilization for the degradation of emerging pollutants in water. *Appl. Catal. B* **2010**, *100*, 338–345. [[CrossRef](#)]
10. Munoz, M.; Zahara, M.D.P.; Casas, J.A.; Rodriguez, J.J. Preparation of magnetite-based catalysts and their application in heterogeneous Fenton oxidation—A review. *Appl. Catal. B* **2015**, *176–177*, 249–265. [[CrossRef](#)]
11. Bae, S.; Kim, D.; Lee, W. Degradation of diclofenac by pyrite catalyzed Fenton oxidation. *Appl. Catal. B* **2013**, *134–135*, 93–102. [[CrossRef](#)]
12. Mirzaei, A.; Chen, Z.; Haghghat, F.; Yerushalmi, L. Removal of pharmaceuticals from water by homo/heterogenous Fenton-type processes—A review. *Chemosphere* **2017**, *174*, 665–688. [[CrossRef](#)] [[PubMed](#)]
13. Zang, H.; Miao, C.; Shang, J.; Liu, Y.; Liu, J. Structural effects on the catalytic activity of carbon-supported magnetite nanocomposites in heterogeneous Fenton-like reactions. *RSC Adv.* **2018**, *8*, 16193–16201. [[CrossRef](#)]
14. Velichkova, F.; Julcour-Lebigue, C.; Koumanova, B.; Dlmaz, H. Heterogeneous Fenton oxidation of paracetamol using iron oxide (nano)particles. *J. Environ. Chem. Eng.* **2013**, *1*, 1214–1222. [[CrossRef](#)]
15. Mehdaoui, R.; El Ghali, A.; Cheikhrouhou, W.; Beyou, E.; Baouab, M.H.V. Fe<sub>3</sub>O<sub>4</sub> nanoparticles coated by new functionalized tetraaza-2,3 dialdehyde micro-crystalline cellulose: Synthesis, characterization, and catalytic application for degradation of Acid Yellow 17. *Iran. Polym. J.* **2017**, *26*, 597–613. [[CrossRef](#)]
16. Kim, D.K.; Mikhaylova, M.; Zhang, Y.; Muhammed, M. Protective Coating of Superparamagnetic Iron Oxide Nanoparticles. *Chem. Mater.* **2003**, *15*, 1617–1627. [[CrossRef](#)]
17. Umar, I.A.; Giwa, A.; Salisu, B.; Sallahudeen, M.; Mustapha, A. Kinetics, equilibrium and thermodynamics studies of C.I. Reactive Blue 19 dye adsorption on coconut shell based activated carbon. *Int. Biodeterior. Biodegrad.* **2015**, *102*, 265–273.
18. Apostol, L.C.; Pereira, L.; Pereira, R.; Gavrilescu, M.; Alves, M.M. Biological decolorization of xanthene dyes by anaerobic granular biomass. *Biodegradation* **2012**, *23*, 725–737. [[CrossRef](#)] [[PubMed](#)]
19. Houas, A.; Lachheb, H.; Ksibi, M.; Elaloui, E.; Guillard, C.; Herrmann, J.-M. Photocatalytic degradation pathway of methylene blue in water. *Appl. Catal. B* **2001**, *31*, 145–157. [[CrossRef](#)]
20. Arivizhivendhan, K.V.; Mahesh, M.; Boopathy, R.; Regina Mary, R.; Sekaran, G. A novel method for the extraction of prodigiosin from bacterial fermenter integrated with sequential batch extraction reactor using magnetic iron oxide. *Process Biochem.* **2016**, *51*, 1731–1737.
21. Chen, G.; Liu, J.; Yao, J.; Qi, Y.; Yan, B. Biodiesel production from waste cooking oil in a magnetically fluidized bed reactor using whole-cell biocatalysts. *Energy Convers. Manag.* **2017**, *138*, 556–564. [[CrossRef](#)]
22. Liang, X.; He, Z.; Zhong, Y.; Tan, W.; He, H.; Yuan, P.; Zhu, J.; Zhang, J. The effect of transition metal substitution on the catalytic activity of magnetite in heterogeneous Fenton reaction: In interfacial view. *Colloids Surf. A* **2013**, *435*, 28–35. [[CrossRef](#)]
23. Wang, N.; Zheng, T.; Zhang, G.; Wang, P. A review on Fenton-like processes for organic wastewater treatment. *J. Environ. Chem. Eng.* **2016**, *4*, 762–787. [[CrossRef](#)]
24. Naimi, I.; Bellakhal, N. Removal of 17β-Estradiol by Electro-Fenton Process. *Mater. Sci. Appl.* **2012**, *3*, 880–886. [[CrossRef](#)]
25. Siddique, M.; Farooq, R.; Price, G.J. Synergistic effects of combining ultrasound with the Fenton process in the degradation of Reactive Blue 19. *Ultrason. Sonochem.* **2014**, *21*, 1206–1212. [[CrossRef](#)] [[PubMed](#)]
26. Bilal, M.; Rasheed, T.; Iqbal, H.M.; Li, C.; Wang, H.; Hu, H.; Wang, W.; Zhang, X. Photocatalytic degradation, toxicological assessment and degradation pathway of CI Reactive Blue 19 dye. *Chem. Eng. Res. Des.* **2018**, *129*, 384–390. [[CrossRef](#)]
27. Fanchiang, J.-M.; Dyi-Hwa, T. Degradation of anthraquinone dye C.I. Reactive Blue 19 in aqueous solution by ozonation. *Chemosphere* **2009**, *77*, 214–221. [[CrossRef](#)] [[PubMed](#)]
28. Massart, R. Preparation of aqueous magnetic liquids in alkaline and acidic media. *IEEE Trans. Magn.* **1981**, *17*, 1247–1248. [[CrossRef](#)]

